36th European Rotorcraft Forum, 2010

# Investigation of Finite Element Approaches for Rotor Blade Structural Dynamics

Khiem-Van Truong*
D.A.D.S
ONERA
Châtillon, France

Hyeonsoo Yeo† Robert A. Ormiston‡
Aeroflightdynamics Directorate (AMRDEC)
U.S. Army Research, Development, and Engineering Command
Ames Research Center, Moffett Field, California

**Abstract**: With configurations of modern rotor blades that depart from the shape of long slender structures or involve rapid variations of planform and cross-sections at the blade root, the question of validity of the classical 1-D beam modeling method is raised. More sophisticated structural models will require 3-D finite elements (FE) such as shells and bricks, but with increased computer memory and run time. The structural complexity of the rotor blade hampers its analysis by the 3-D FE method, as the number of degrees of freedom (dofs) sufficient to accurately model the blade is expected to be very high, on the order of millions. This study investigates modeling assumptions for 3-D FE analysis in order to establish a rotor blade model with manageable memory size and run time. This is done through a systematic comparison of predictions of 1-D and 3-D methods in several problems ranging from simple isotropic beams to realistic composite blades with straight planform and length sufficiently high, so that 3-D effects are negligible. Natural frequencies are calculated at various rotor angular speeds and correlated with experimental results for various test cases. Accuracy of both 1-D and 3-D methods has also been assessed through analysis of discretization errors that originate from insufficiently refined meshing.

## 1. Introduction

Rotorcraft aeromechanics analysis is a challenging problem due to coupling of the complex structural deformations of rotor blades with the three dimensional and highly unsteady aerodynamic environments. Rotorcraft comprehensive analyses [1–5] have been widely used to model a broad spectrum of rotorcraft attributes, including performance, airloads, structural loads, air flow fields, and hub loads. Most rotorcraft comprehensive analysis codes use 1-D beam elements for rotor blade dynamics modeling. Traditional approaches rely on the fact that rotor blades are typically long slender structures with slowly varying elastic properties. This enables the splitting of the 3-D analysis into 1-D and 2-D analyses, resulting into 1-D beam theory with cross-section beam characteristics calculated by a 2-D code. This method is efficient and accurate as long as the cross sections are small compared to the wave-length of deformations along the beam and the initial curvatures and twists. Modern rotor blades have begun to depart from simple straight planform by incorporating tip sweep and taper. For example, deviations from the classical rectangular shape in order to significantly reduce noise generated by blades led to the research ERATO blade and recently to the industrial "Blue Edge" blade. Cantilever (hingeless, bearingless) blades involve planform and cross-section variations at the blade root. Use of composite material also complicates analysis due to material anisotropy. Such configurations raise the question of validity of 1-D beam method. More sophisticated structural models will require 3-D finite elements (FE) such as shells and bricks, but with increased computational demands in both computer memory and run time. The structural complexity of the rotor blade hampers its analysis by the 3-D FE method, as the number of degrees of freedom sufficient to accurately model the blade is expected to be very high [6] , on the order of millions. Interested readers are referred to recent efforts [7] to develop a parallel and scalable solution procedure for a 3-D FE model based rotor dynamics analysis.

The US Army Aeroflightdynamics Directorate (AFDD) and the French Office National d'Etudes et de Recherches Aérospatiales (ONERA) have been conducting research to investigate the differences between a 1-D beam model approach and a 3-D FE approach under the auspices of the United States/France Memorandum of Agreement (MoA) on Helicopter Aeromechanics. The objective of this effort is to better understand the accuracy of current rotor blade structural modeling and identify the level of sophistication required to model modern rotor blades, i.e. to determine

*Research Scientist, Khiem-Van.Truong@onera.fr
†Research Scientist, hyeonsoo.yeo@us.army.mil
‡Chief Scientist, Aeromechanics, robert.ormiston@us.army.mil

when the use of 3-D method will be necessary. AFDD conducts 1-D beam analysis using Rotorcraft Comprehensive Analysis Systems (RCAS) with sectional properties calculated from Variational Asymptotic Beam Sectional Analysis (VABS) [8,9]. ONERA elaborates model meshing with MSC/Patran and conducts 3-D FE analysis with MSC/Marc. Initial results have been published recently |10] on the predictions of 1-D and 3-D methods of natural frequencies of various blades, ranging from simple beams to a realistic blade. The differences between the two analyses have been quantified and effects of blade length have been reported. However, details have not been provided on the accuracy attained in both methods for modeling rotor blade structural dynamics, particularly in the 3-D FE procedure implemented. 3-D FE analysis is a rather mature technique applied to various fields (fixed wing aircraft, automobile,…) but it is not yet validated for modeling helicopter rotor blades.

The main concern of this communication is to show that it is feasible to make a 3-D FE model of rotor blade with a reasonable number of degrees of freedom (dofs), on the order of some hundreds of thousands. A higher number of dofs is not manageable with present computer memory size and run time. The US/French MoA collaboration has provided the opportunity for a thorough examination of various 3-D modeling assumptions, important for a better simulation of rotor blade structural dynamics.

## 2. Overview of test cases studied

The study is directed towards a realistic rotor blade based on a simplification of the straight ADM (**A**dvanced **D**ynamics **M**odel) blade tested by AFDD for aeroelastic stability [11]. The rotor is 7.5 feet in diameter and has a chord c = 3.4 in. The blade, shown in Figure 1, contains three sections: a flexure section, a transition section and a lifting part characterized by a constant cross-section. The geometry of the lifting cross-section is shown in Figure 2: the airfoil is a NACA 0012 without twist; the internal components are comprised of a spar made of unidirectional fiber, a high density leading edge and two kinds of foams enclosed by multi-layer composites with various compositions and thicknesses. At the blade skin, there are three multilayer composites with different thicknesses, as enlarged in Figure 2. The detailed blade materials and geometry are listed in Tables 1 and 2.

The simplified blade is comprised of a rigid beam (hypothetic material with Young's modulus E= 1000 GPa) of length equal to 3 chords (3c) connected to the lifting section of length equal to 20 chords (Figure 3), it will be denoted as the ADM* blade. Thus, flexure and transition sections are not represented in the model. Effects of non-rectangular sections like transition on the dynamic behavior of the blade are considered in an ongoing study. The length of 20 chords is considered as sufficiently long, to ensure that 3-D effects are negligible [10]. The ADM* blade, although based on a simplification of the straight ADM blade, contains all the ingredients of a realistic blade: shape of an airfoil for the cross–section, material composition involving isotropic, orthotropic solids, and composites. Test cases have been built to reflect this composition (cf. Table 3) and also to make use of existing experiments for correlation studies between experimental results and predictions of the two analyses, except for test cases 2 and 7 (realistic blade). Test case 2 corresponds to a foam blade that is not practical for rotor blade application but it is used to investigate the importance of materials on 3-D effects. All the cases studied have ratio of beam length to chord greater than 18, i.e. sufficiently high for 3-D effects associated with beam length to be negligible.

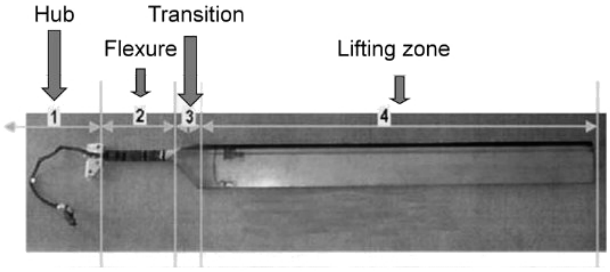


*Figure 1. The ADM blade: it contains three main parts, flexure, transition and lifting sections.*

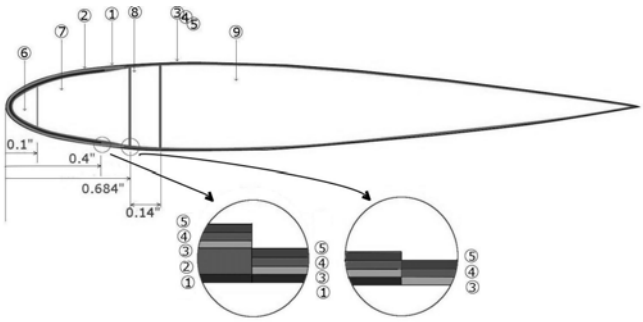


*Figure 2. ADM blade cross section geometry: the various components are described in Tables 1 and 2.*

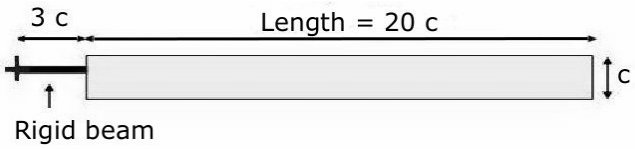


*Figure 3. The realistic blade, based on a simplification of the straight ADM blade.*

## 3. Convergence studies of 1-D and 3-D methods

The question of accuracy in the predictions of the dynamic behavior of a rotor blade based on 1-D and 3-D methods is not thoroughly investigated in papers related to the subject. There are various sources of errors for both analyses. Besides the obvious misuse of the codes, there are discretization errors originating from insufficiently refined meshing of the model.

*1-D beam analysis*

The 1-D analysis is preceded by a 2-D analysis that provides beam cross-section characteristics. AFDD uses a geometrically exact, shear flexible, anisotropic beam element implemented in the Rotorcraft Comprehensive Analysis System (RCAS). The geometrically exact composite beam element (GCB) is specifically intended for composite blades and it is designed to be compatible with Variational Asymptotical Beam Sectional Analysis (VABS) [8,9], a code developed by Cesnik, Hodges, and their co-workers at Georgia Institute of Technology for determining beam cross-section elastic and mass constants. Discretization errors may occur at two levels: insufficient number of beam elements and insufficient number of elements for VABS calculations. The test case considered for convergence studies is a cantilevered ADM* blade without the rigid beam and length L = 10c.

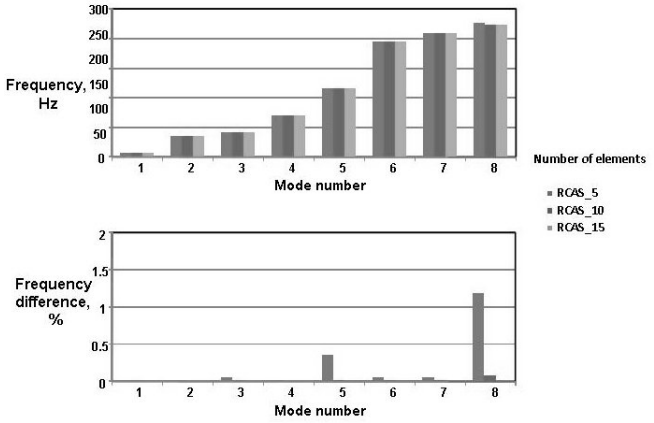


*Figure 4. Effects of the number of beam elements on the values of natural frequencies of the cantilevered ADM* blade L = 10c*

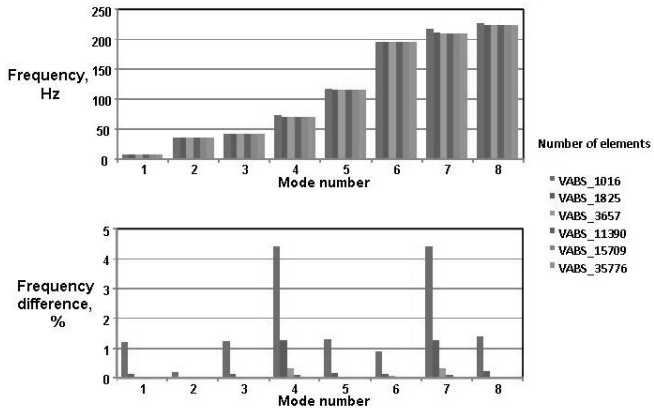


*Figure 5. Effects of the number of triangular elements in the cross-section for VABS calculations on the values of natural frequencies of the cantilever ADM* blade L = 10c.*

Effects of the number of beam elements on the values of natural frequencies of the blade are reported in Figure 4: a number of 10 beam elements shows good convergence of results with less than 0.1% of relative error. Effects of meshing the cross-section for VABS on the values of natural frequencies are displayed in Figure 5: a number greater than 4000 triangular elements shows accurate results within less than 0.1% relative error.

*3-D FE analysis*

For the generation of meshes, ONERA uses the commercial code MSC/Patran and for 3-D finite element analysis MSC/Marc and in some circumstances MSC/Nastran for verification. MSC/Marc is a nonlinear finite element code that provides capabilities for studying dynamic structures undergoing large deformations and it includes both geometric and material nonlinearities. It is not a code dedicated to rotating structures studies, but is a general-purpose code for simulating a wide range of engineering

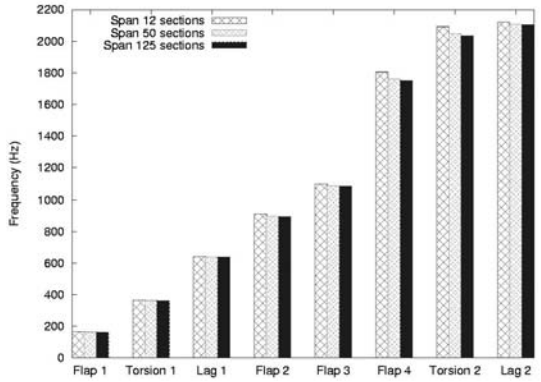


*Figure 6a*

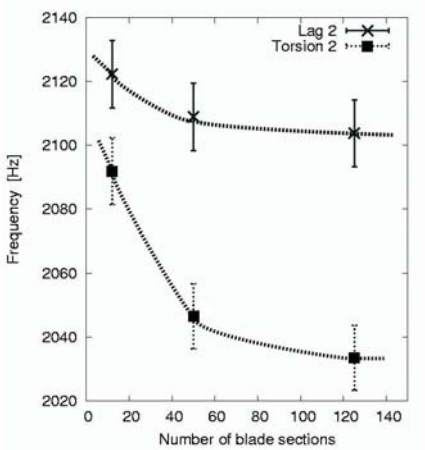


*Figure 6b*

*Figure 6. Effects of the number of subdivisions of the blade span on the values of natural frequencies of the cantilever ADM* blade L =2c:*
*a. Effects on the first eight modes according to models 1-3;*
*b. Convergence of two modes, the second lag mode and the second torsion mode, versus the number of subdivisions of the ADM*blade span. The error bar corresponds to ±0.5% of relative error.*

applications and manufacturing processes. It also can be tailored to user needs, through user defined subroutines written in Fortran. The crux of the problem in FEA is to get a mesh that satisfactorily balances accuracy and computing

resources. Convergence studies are carried out on a cantilever ADM* blade, without a hub and with a shorter blade length of two chords (2c). It is not possible to perform it on a blade with L=10c, due to the amount of computer memory involved, as it is needed to increase the number of nodes by tenfold for getting meaningful convergence results.

The basic meshing of the ADM* blade cross-section requires at least 182 nodes, such a typical configuration is obtained through observation of constraints on the dimensions of elements used and a modeling simplification that will be explained in section 4, to take care of difference of composite thicknesses at the blade skin. In FE analysis, there are constraints on the element dimensions, it is usually recommended that the aspect ratio $R_t$ (ratio of the largest dimension over the smallest dimension) for brick elements should not be much larger than 10, for shells and solid shells, the aspect ratio may be higher.

Refining meshing can be done either along the blade span or in the cross-section. Effects of refining meshing according to the first way are examined by dividing the reference blade with 182 nodes in the cross-section into 12, 50 and 125 spanwise sections corresponding to models 1, 2 and 3 respectively, in Figure 6. Such subdivisions of the blade corresponds to varying aspect ratio $R_t$ of brick elements through values 44.2, 10.6 and 4.1 respectively, as the smallest dimension of brick elements in the model is 0.326 mm. Effects associated with the variations of $R_t$ on natural frequencies of the cantilevered ADM* blade with L=2c are shown in Figures 6a and 6b: if 0.5% of relative error in discretization is allowed, a value of $R_t$ of about 20 is acceptable. The effects of refining meshing in the cross-section are then examined: starting from a reference model (model 1) with 182 nodes in the cross-section and 50 sections along the span, two models (models 2, 3) are elaborated with 538 and 1068 nodes respectively (Figure 7a). The effects on natural frequencies are reported in Figures 7b and 7c: a number of 182 nodes in the cross-section is acceptable for less than 0.5% of relative error from discretization.

The conclusions reached in this section will be used in the study of different test cases discussed in section 4.

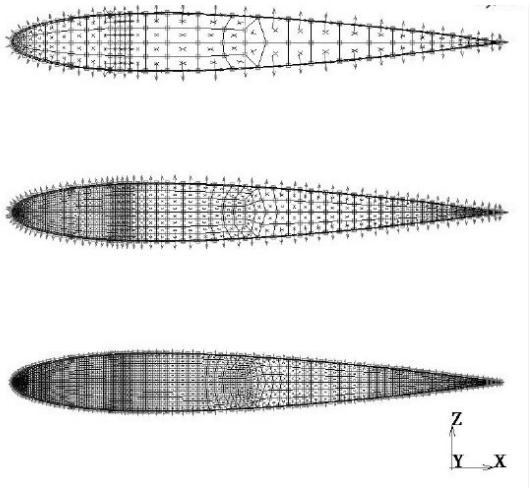


*Figure 7a*

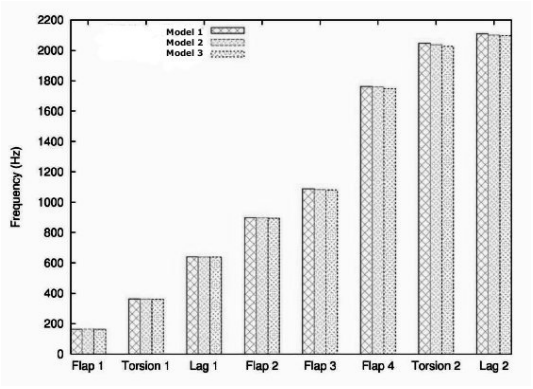


*Figure 7b*

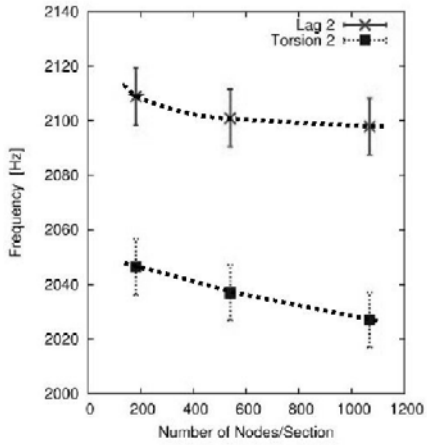


Figure 7c

*Figure 7. Effects of refining meshes in the cross-section on the values of natural frequencies of the cantilever ADM* blade with L=20c:*
*a. Various models 1-3 from top to bottom;*
*b. Effects on the first eight modes according to models;*
*c. Convergence of two modes, the second lag mode and the second torsion mode, versus the number of nodes in the cross-section. The error bar corresponds to ±0.5% of relative error.*

## 4. Results and discussions

Comparisons between the 1-D and 3-D analyses are conducted first for materials similar to constituents of the ADM* blade (isotropic, orthotropic and composite, detailed in Table 3) before the ADM* blade, in order to better understand the differences between the two analyses.

### *4.1 Isotropic blades (Cases 1-2)*

The first test case concerns an aluminium beam of L=40 in, including a 2.5-in "hub", the width of the cross-section is 1.0 in and the thickness is 0.0633 in. The beam configuration is depicted in Figure 8. It was investigated experimentally by University of Maryland [12]. The Young's modulus is E = 1.0E+07 lb/in$^2$ (68.9 GPa), Poisson's ratio is $\nu$ = 0.3, and the mass density is $\rho$ = 2.538E-04 lb-sec$^2$/in$^4$ (2713 kg/m$^3$). RCAS uses 15 elements; one rigid bar element to model the hub and 14 beam elements to model the beam. The cross-sectional properties were obtained from VABS using 9-noded

quadrilateral elements. In the 3-D finite element analysis, the hub is modeled by a rigid beam (material with high value of Young's modulus) and the aluminium beam by 8-noded brick elements (1800 elements) as shown in Figure 9. MSC Software has recommended, in its user's manual, linear 3-D elements rather than quadratic 3-D elements. For the 3-D FE analysis, the connection between the rigid beam and the elastic portion is not straightforward as for the 1-D beam analysis. The solution adopted is to connect all the nodes of the first section of the blade (near the root) to the centre node C through rigid links using a rigid body element RBE2 involving all degrees of freedom (dofs). In such a rigid link, the node C plays the role of master node and the nodes connected to it are slave nodes for all dofs (3 translations in this case, however, it is possible to restrict RBE2 link to some determined dofs).

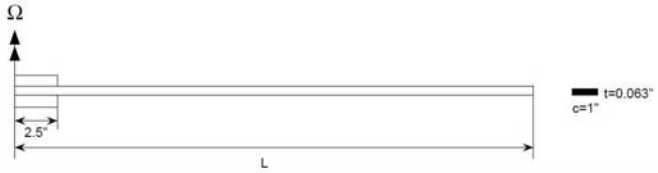


*Figure 8. Beam configuration of test case 1.*

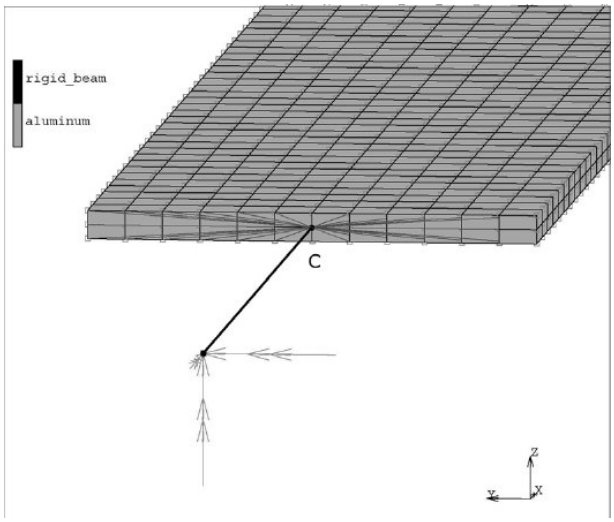


*Figure 9. 3-D mesh for beam configuration 1.*

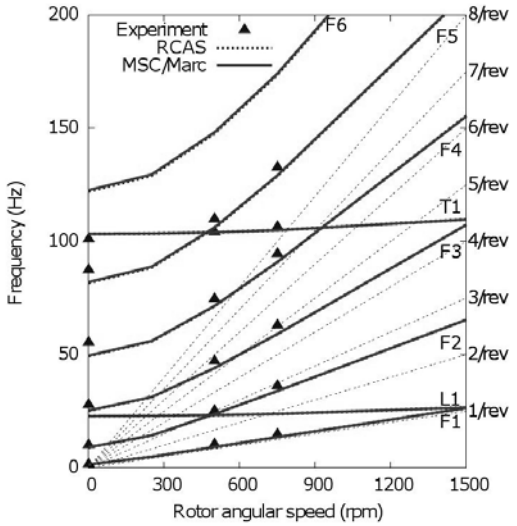


*Figure 10. Frequency comparison for aluminum beam.*

The natural frequencies calculated with the two analyses are compared with experimental data in Figure 10. Experimental frequency measurements were made up to 750 RPM. However, analytical calculations are extended to 1500 RPM, more representative of rotor angular speed value. Comparisons are made for up to 8 modes in this figure and throughout the paper. The two analyses show identical results and good agreement with experiments. The modeling conjecture of 3-D FE analysis for connecting a rigid beam to the blade performs correctly.

A beam made of foam is considered in test case 2. The geometric configuration is simplified from the first test case with the elimination of the rigid beam. The length of the beam is equal to 20c, its cross-section is c x c/4, with c = 3.4 in, Figure 11. The Young's modulus is E = 1.1995E+04 lb/in$^2$ (0.0827 GPa), the shear modulus is G = 4.9978E+03 lb/in$^2$ (0.0344 GPa) and the mass density is $\rho$ = 1.7871E-05 lb-sec$^2$/in$^4$ (190.99 kg/m$^3$). The material properties are substantially different from those of aluminum. Figure 12 shows the modal frequency comparison for rotor angular speeds up to 1700 rpm. There is good agreement between the two analyses: natural frequencies predicted have relative differences less than 1%, except for the first torsion frequency where RCAS predicts about 1.5% lower than MSC/Marc.

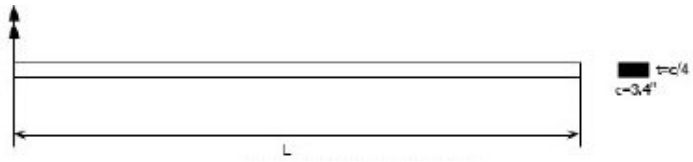


*Figure 11. Beam configuration for test case 2.*

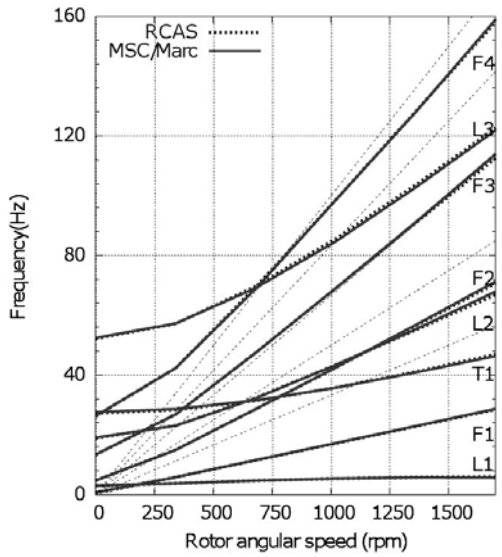


*Figure 12. Frequency comparison for foam blade.*

### *4.2 Composite blades*

#### *4.2.1 Non-rotating composite beams (Cases 3-4)*

One important material constituent of the blade is multilayer composite. The MSC/Marc code provides various elements for modeling composites: thick shells with 4 nodes, brick elements with 8 and 20 nodes and, recently, solid shells with 8 nodes [13]. Thick shells are traditionally preferred for their simplicity to set up and for their robust numerical convergence. The new solid shell is interesting to use: according to MSC Software, it requires less CPU time than classical bricks and takes better account of bending behavior than thick shells.

Static and dynamic behaviors of structurally coupled composite beams with rectangular section were investigated by Minguet and Dugundji [14, 15]. Several types of beams were manufactured from AS4/3501-6 graphite/epoxy and tested dynamically to measure natural frequencies and mode shapes. Their deflection under gravity was also measured. The AS4/3501-6 ply properties are: $E_1$ = 2.060E+07 lb/in$^2$ (142.0 GPa), $E_2 = E_3$ =1.420E+06 lb/in$^2$ (9.8 GPa), $G_{12} = G_{23} = G_{13}$ = 8.700E+05 lb/in$^2$ (6.0 GPa) , $\nu_{12} = \nu_{13}$ = 0.42, $\nu_{23}$ = 0.54 and mass density $\rho$ = 1.440E-04 lb-sec$^2$/in$^4$ (1538 kg/m$^3$) [15]. Two multilayer composite sections were investigated in the present study: $[20\circ/-70\circ/-70\circ/20\circ]_{2a}$ and $[45\circ/0\circ]_{3s}$ , with layup thicknesses of 1.92 mm and 1.47 mm respectively. Due to high temperature treatment during fabrication, the material characteristics change and, in practice, such global change is taken into account by varying the sample thickness in order to match the static deflection under gravity or under tip loading. In this case, the mass density is changed to match the deflection under gravity and is equal to 1.385E-04 lb-sec$^2$/in$^4$ (1480 kg/m$^3$) and 1.544E-04 lb-sec$^2$/in$^4$ (1650 kg/m$^3$) respectively [16], instead of the original value of 1.44E-04 lb-sec$^2$/in$^4$ (1538 kg/m$^3$). The exact values of material characteristics appear to be crucial for correlation studies but generally they are not well documented.

The first layup has extension-twist coupling and the second one has bending-twist coupling. The beams were cantilevered in the test fixture and non-rotating frequencies were measured. Blade natural frequencies are calculated with MSC/Marc code using two models based on thick shells and solid shells respectively. They are compared with experiment in Tables 4 and 5. For the extension-twist coupled beam, the two elements of MSC/Marc provide the same predictions but consistently lower than the experimental results. MSC/Marc predictions are better correlated to the experimental results than the RCAS analysis, this latter shows substantial underprediction of the torsion frequency (5.3%). For the bending-twist coupled beam, the solid shell in MSC/Marc provides a better prediction than the thick shell but the analysis is not in good agreement with experiments: overprediction of frequencies of flap modes (5.2 % for third flap mode) and underprediction of torsion frequency (3.4%). The 1-D analysis shows results similar to the 3-D analysis with solid shells. Based on this study, the solid shell will be used for the remainder of the study with MSC/Marc.

#### *4.2.2 Rotating composite beams (Cases 5-6)*

Graphite-epoxy beams were tested in the University of Maryland vacuum chamber [12]. Two layup angles were examined: Case 5 ($[0^o]_{24}$) and Case 6 ($[15^o]_{24}$). The beam tested has a length L = 40 in with a 2.5-in "hub". The width of the cross-section is equal to 1.0 in, same as the aluminium beam tested (configuration 1 shown in Figure 8). The sample thicknesses are 0.117 in and 0.120 in, respectively. The material characteristics used are as listed in the previous section (AS4/3501-6 ply properties). It should be noted that there is no coupling between modes for the $[0^o]_{24}$ case. However, there is flap-torsion coupling due to angle-ply lay-up for the $[15^o]_{24}$ case. In the 3-D analysis, the beam is meshed with solid shells. Again, the 1-D and 3-D analyses show almost identical results and good correlation with experiment, as shown in Figures 13 and 14. For the $[0^o]_{24}$ lay-up case, there is good agreement between the two

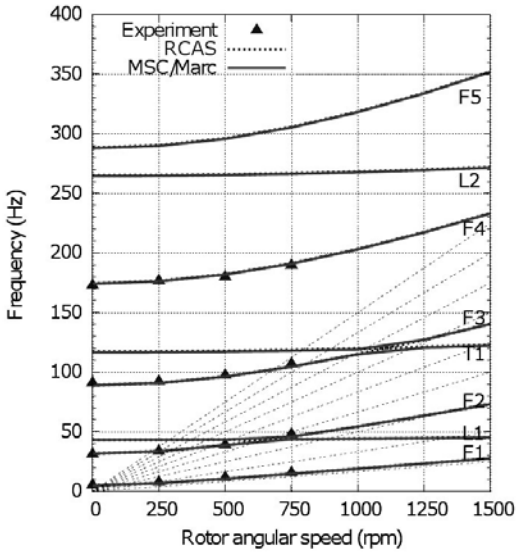


*Figure 13. Frequency comparison for graphite-epoxy beam $[0^o]_{24}$ lay-up.*

approaches. For the $[15^o]_{24}$ case, there are small but visible differences between the two approaches. The differences appear in the flap modes and the differences become larger for higher frequency modes: 1.5% for the fourth flap mode. It is probably the torsion that causes the difference, due to the flap-torsion coupling as discussed in Ref. 10.

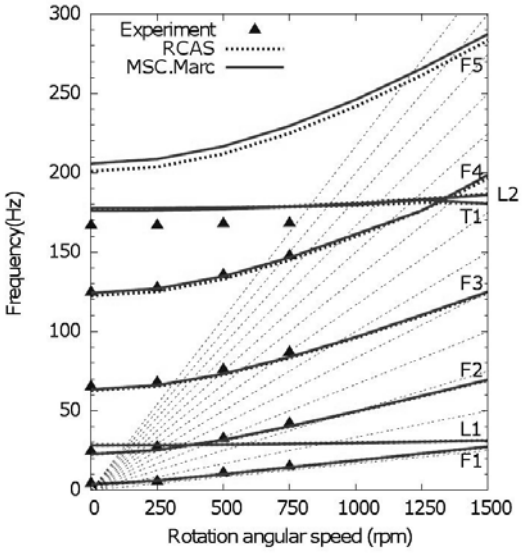


*Figure 14. Frequency comparison for graphite-epoxy beam $[15^o]_{24}$ lay-up.*

### *4.3. ADM* blade (Case 7)*

The materials and geometry of the ADM* blade are listed in Tables 1 and 2. Some of material properties were not known, and thus assumed values were used in the analyses. Properties of components 3 and 4, corresponding to fiber glass plys of ($0^o$ / $90^o$) and ($+45^o$ / $-45^o$) respectively, should be provided by those of a unique ply. For orthotropic materials (components 1-5, 7 and 8), the various components of shear modulus and Poisson's ratios according to different axes are assumed equal, although their values should be different. Important variation occurs for the components of Poisson's ratio, usually $\nu_{23}$ is important compared to $\nu_{12}$ and $\nu_{13}$. Note that the input values for MSC/Marc are $\nu_{12}$ , $\nu_{23}$ and $\nu_{31}$ ( = $\nu_{13}$ $E_3/E_1$, different from $\nu_{13}$). For this study, based on comparison between two analyses, it is not important to have correct values of material characteristics as long as the two analyses use the same properties, but it will not be the case for correlation studies with experiments.

The meshing of this blade, as for other real blades, raises some concern at the boundary region between two composites of different thicknesses at the blade. The origin of the meshing problem can be explained by referring to Figure 15: the various composites wrapping the blade have different thicknesses (Figure 2) and at the boundary of two different composites, the interior nodes A and B are not at the same geometric position. For FE analysis, at the boundary denoted by "BS" in Figure 15, meshes must be topologically congruent (coincident), i.e. nodes A and B must be shared nodes at the interface. The distance AB is usually small, less than tenths of a millimeter, and if an element with edge AB is created, the number of nodes in a cross-section will increase to thousands due to the constraint on the aspect ratio of elements and, therefore, the total number of nodes for the model could reach millions. The solution advocated in this study is to link node A to node B by a rigid link RBE2 involving all dofs. Using this modeling simplification, it is possible to mesh the ADM blade cross-section with 182 nodes. For the ADM* blade with length L=20c, it is possible to mesh with about 46000 nodes, by using an aspect ratio of brick elements of about 20. Notice that real rotor blade usually has a shorter length.

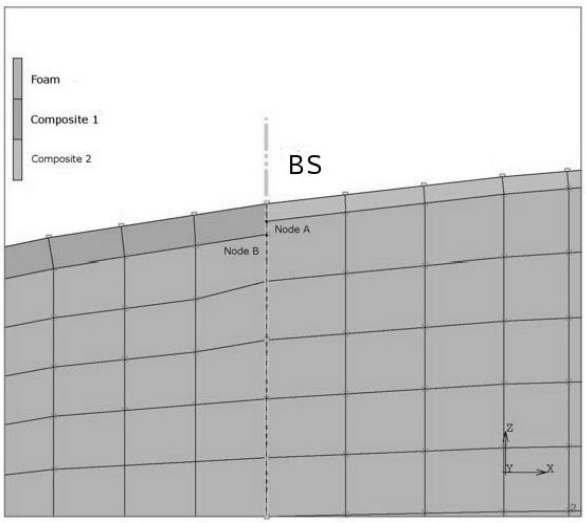


*Figure 15. Boundary region between two composites of different thicknesses at the skin of a rotor blade*

The predictions obtained are compared to those of 1-D beam analysis for the blade with length L = 20c in Figure 16. The two analyses agree within a few percent of relative error, predicted flap modes are in good agreement. The most visible difference between the two analyses occurs for the second torsion mode, about 2% (cf. Table 6), but it is in the same order of differences for the first torsion mode and the first two lag modes. A careful check of material properties was made by both partners and the only remaining difference seems to be in a different modeling of the zone of the trailing edge of the blade.

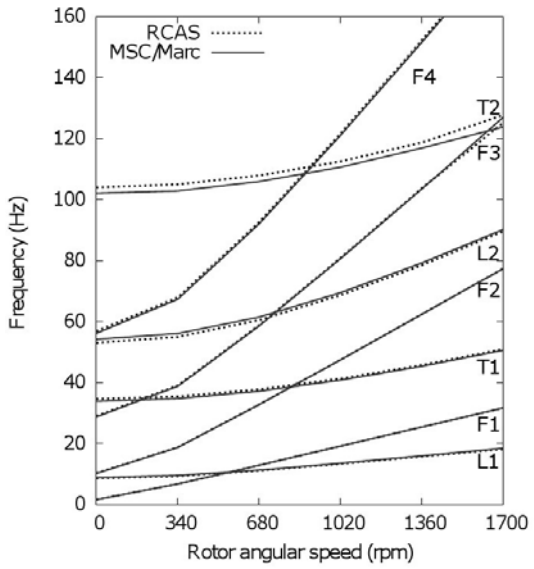


*Figure 16. Frequency comparison for ADM* blade with length L=20*c

## 5. Concluding Remarks

Through a systematic comparison of predictions of 1-D and 3-D methods and correlation with existing experimental results, various modeling assumptions for 3-D FE analysis have been tested:

- assessing the mesh dimension through analysis of discretization errors, note that is also done for the 1-D beam analysis;
- connection between beam and solids;
- use of appropriate finite elements (solid shells) for modeling multilayer composites at the blade skin;
- simplification for meshing composites differing by thicknesses at the blade skin.

From this study, following conclusions were obtained:

- In general, there is good agreement between the 1-D and 3- D analyses for the test cases where the beam length is sufficiently long, as expected.
- The connection between beam and brick elements using a rigid link (rigid body element RBE2) and a master node provides an adequate boundary condition.
- The solid shell element shows better natural frequency correlation than the thick shell element for the analysis of multilayer composites.
- Connecting two composite layers with different thicknesses using a rigid link significantly reduces the number of meshes required.

The modeling guidelines that are drawn from this study could be used for 3-D FE modeling of helicopter rotor blade to obtain model size and run time manageable, some hundreds of thousands of dofs. This basic study will permit the consideration of 3-D effects associated with deviations of blade planform to the classical rectangular shape and rapid variations of planform and material properties at the blade root.

These modeling assumptions will be used by ONERA for coupling high fidelity CSD (Computational Structural Dynamics) techniques with CFD (Computational Fluid dynamics).

## 6. Acknowledgements

The authors would like to express thanks to Mr. Tom Maier of AFDD for providing detailed section geometry and material properties of the ADM blade.

## 7. References

[1]Saberi, H. A., Khoshlahjeh, M., Ormiston, R. A., and Rutkowski, M. J., "RCAS Overview and Application to Advanced Rotorcraft Problems," AHS Fourth Decennial Specialists' Conference on Aeromechanics, San Francisco, CA, January 21-23, 2004.

[2]Johnson, W., "Rotorcraft Dynamics Models for a Comprehensive Analysis," AHS International 54th Annual Forum Proceedings, Washington D.C., May 20-22, 1998.

[3]Bauchau, O. A. and Kang, N. K., "A Multibody Formulation for Helicopter Structural Dynamic Analysis," *Journal of the American Helicopter Society*, Vol. 38, No. 2, April 1993, pp. 3-14.

[4]Bir, G. and Chopra, I., "University of Maryland Advanced Rotor Code (UMARC) Theory Manual," Technical Report UM-AERO 94-18, Center for Rotorcraft Education and Research, University of Maryland, College Park, July 1994.

[5]Dequin, A. M., Benoit, B., Kampa, K., von Grünhagen, W., Basset, P. M., and Gimonet, B., "HOST, a General Helicopter Simulation Tool for Germany and France," American Helicopter Society 56th Annual Forum, Virginia Beach, VA, May 2-4, 2000.

[6]Hill, G.F.J and Weaver, P.M.., "Structural Properties of Helicopter Rotor Blade Sections," 28th European Rotorcraft Forum, Bristol, United Kingdom, September 17-20, 2002.

[7]Datta, A. and Johnson, W., "A Multibody Formulation for Three Dimensional Brick Finite Element Based Parallel and Scalable Rotor Dynamic Analysis," American Helicopter Society 66th Annual Forum, Phoenix, AZ, May 11-13, 2010.

[8]Cesnik, C. E. S. and Hodges, D. H., "VABS: A New Concept for Composite Rotor Blade Cross-Sectional Modeling," *Journal of the American Helicopter Society*, Vol. 42, No. 1, January 1997, pp. 27-38.

[9]Hodges, D.H., "Nonlinear Composite Beam Theory," Progress in Astronautics and Aeronautics, Vol. 213, 2006.

[10] Yeo, H., Truong,V.K. and Ormiston, R.A., "Assessment of 1-D Versus 3-D Methods for Modeling Rotor Blade Structural Dynamics," 51st AIAA/ASME/ASCE/AHS/ASC Structures, Structural Dynamics, and Materials Conference, Orlando, FL, April 12-15, 2010.

[11] Maier T. A., Sharp, D. L., and Abrego, A. I., "Aeroelastic Stability for Straight and Swept-Tip Rotor Blades in Hover and Forward Flight," American Helicopter Society 55th Annual Forum Proceedings, Montreal, Canada, May 25-27, 1999.

[12]Epps, J. J. and Chandra, R., "The Natural Frequencies of Rotating Composite Beams with Tip Sweep," *Journal of the American Helicopter Society*, Vol. 41, No. 1, January 1996, pp. 29-36.

[13] Cardoso, R.P.R., Malerdika, M., Chaudhry, S., Alves de Souza, R.J. and Valente, R.A.F., "Enhanced Assumed Strain (EAS) and Assumed Natural Strain (ANS) Methods for

One-point Quadrature Solid-Shell Elements," *International Journal for Numerical Methods in Engineering*, Vol. 75, 2008, pp. 156–187
[14] Minguet, P. and Dugundji, J., "Experiments and Analysis for Composite Blades Under Large Deflections Part I: Static Behavior," *AIAA Journal*, Vol. 28, No. 9, September 1990, pp. 1573-1579.
[15] Minguet, P. and Dugundji, J., "Experiments and Analysis for Composite Blades Under Large Deflections Part II: Dynamic Behavior," *AIAA Journal*, Vol. 28, No. 9, September 1990, pp. 1580-1588.
[16] Hodges, D. H., Atilgan, A. R., Fulton, M. V. and Rehfield, L. W., "Free-Vibration Analysis of Composite Beams," *Journal of the American Helicopter Society*, Vol. 36, 1991, pp. 36-47.

**Table 1. ADM rotor blade materials and geometry**

| **Component** | **Material** |
|---|---|
| Component 1 | 0.002-inch thick E-1002 fiberglass skin +45˚/-45˚ (0.684 inch in chord direction) |
| Component 2 | 0.006-inch thick Carbon Graphite leading edge wrap (0.400 inch in chord direction) |
| Component 3 | 0.002-inch thick E-1002 fiberglass skin 0˚/90˚ |
| Component 4 | 0.002-inch thick E-1002 fiberglass skin +45˚/-45˚ |
| Component 5 | 0.002-inch thick E-1002 fiberglass skin 0˚/90˚ |
| Component 6 | Tantalum leading edge slugs |
| Component 7 | 1.7871E-05 lb sec$^2$/in$^4$ foam |
| Component 8 | Fiberite HY-E 9048A1F spar (0.14 in x 0.371 in) unidirectional along span direction |
| Component 9 | 8.9343E-06 lb sec$^2$/in$^4$ foot foam |

**Table 2. Material properties of ADM rotor blade**

| **Component** | **Density** | **$E_1$** | **$E_2$** | **$E_3$** | **$G_{12}=G_{13}=G_{23}$** | **$\nu_{12}=\nu_{13}=\nu_{23}$** |
|---|---|---|---|---|---|---|
| | **lb sec$^2$/in$^4$**<br>**Kg/m$^3$** | **lb/in$^2$**<br>**GPa** | **lb/in$^2$**<br>**GPa** | **lb/in$^2$**<br>**GPa** | **lb/in$^2$**<br>**GPa** | |
| Component 1 and 4 | 1.5976E-04<br>1707.29 | 1.6150E+06<br>11.135 | 1.6150E+06<br>11.135 | 8.0750E+05<br>5.5675 | 6.6079E+05<br>4.556 | 0.46 |
| Component 2 | 1.3470E-04<br>2.7932 | 2.0069E+07<br>137.9 | 1.2993E+06<br>8.96 | 1.2993E+06<br>8.96 | 5.0299E+05<br>3.468 | 0.30 |
| Component 3 and 5 | 1.5976E-04<br>1707.29 | 2.2769E+06<br>15.699 | 2.2769E+06<br>15.699 | 1.1385E+6<br>7.8495 | 3.9662E+05<br>2.7346 | 0.18 |
| Component 6 | 1.2804E-03<br>13683.0 | 2.0972E+05<br>1.446 | 2.0972E+05<br>1.446 | 2.0972E+05<br>1.446 | 7.2292E+04<br>0.4984 | 0.49 |
| Component 7 | 1.7871E-05<br>190.99 | 1.1995E+04<br>0.0827 | 1.1995E+04<br>0.0827 | 1.1995E+04<br>0.0827 | 4.9978E+03<br>0.034458 | 0.20 |
| Component 8 | 1.7094E-04<br>1826.86 | 5.1860E+06<br>35.756 | 2.2375E+06<br>15.427 | 2.2375E+06<br>15.427 | 5.6594E+05<br>3.902 | 0.27 |
| Component 9 | 8.9343E-06<br>95.48 | 4.5034E+03<br>0.03105 | 4.5034E+03<br>0.03105 | 4.5034E+03<br>0.03105 | 1.0000E+03<br>0.012938 | 0.45 |

**Table 3: Blade geometries and materials investigated**

| Case | Material | Cross-section geometry | Length |
|---|---|---|---|
| Case 1 | aluminium | rectangle (1.0 in × 0.063 in) | L = 40×c with 2.5-in hub |
| Case 2 | foam | rectangle (3.4 in × 0.85 in) | L = 20×c |
| Case 3 | composite, $[20^\circ/-70^\circ/-70^\circ/20^\circ]_{2a}$ | rectangle (1.181 in × 0.0756 in) | L = 18.7×c |
| Case 4 | composite, $[45^\circ/0^\circ]_{3s}$ | rectangle (1.181 in × 0.0579 in) | L = 18.7×c |
| Case 5 | composite, $[0^\circ]_{24}$ | rectangle (1.0 in × 0.117 in) | L = 40×c with 2.5-in hub |
| Case 6 | composite, $[15^\circ]_{24}$ | rectangle (1.0 in × 0.117 in) | L = 40×c with 2.5-in hub |
| Case 7 | various composite layers | NACA 0012 (3.4 in × 0.408 in) | L = 20×c with 3c hub |

**Table 4: Frequency comparison for the non-rotating composite beam, $[20^o/-70^o/-70^o/20^o]_{2a}$**

| Mode | Experiment | MSC/Marc | MSC/Marc | RCAS/VABS |
|---|---|---|---|---|
| | | Thick shells | Solid shells | |
| Flap1 | 5.8 | 5.43 | 5.45 | 5.36 |
| Flap2 | 36.0 | 34.02 | 34.02 | 33.34 |
| Flap3 | 103.0 | 95.27 | 95.28 | 92.29 |
| Torsion1 | 166.0 | 159.75 | 160.00 | 156.42 |

**Table 5: Frequency comparison for the non-rotating composite beam, $[45^o/0^o]_{3s}$**

| Mode | Experiment | MSC/Marc | MSC/Marc | RCAS/VABS |
|---|---|---|---|---|
| | | Thick shells | Solid shells | |
| Flap1 | 4.3 | 4.70 | 4.70 | 4.69 |
| Flap2 | 28.0 | 29.39 | 29.39 | 29.35 |
| Flap3 | 78.0 | 82.24 | 82.27 | 82.07 |
| Torsion1 | 135.0 | 125.85 | 130.47 | 130.06 |

**Table 6: Frequency comparison for the non-rotating ADM* blade**

| Mode | RCAS/VABS | MSC/Marc | Difference % |
|---|---|---|---|
| Lag 1 | 1.6651 | 1.647 | 1.1 |
| Flap 1 | 8.7147 | 8.918 | -2.3 |
| Flap 2 | 10.421 | 10.309 | 1.1 |
| Torsion 1 | 34.674 | 33.920 | 2.2 |
| Flap 3 | 29.118 | 28.797 | 1.1 |
| Lag 2 | 53.098 | 54.252 | -2.2 |
| Flap 4 | 56.884 | 56.233 | 1.1 |
| Torsion 2 | 104.020 | 102.111 | 1.8 |